Local Frequency Estimation in Interferograms Using a Multiband Pre-Filtering Approach

Diego Perea-Vega and Ian Cumming

Radar Remote Sensing Group
Dept. of Electrical and Computer Engineering
University of British Columbia
Vancouver, BC Canada V6T 1Z4

Abstract: In this work, we propose a new algorithm for local frequency estimation in which the interferogram signal is pre-filtered *before* the local frequency estimation is performed. This allows the use of a simpler and more efficient frequency estimator that operates at the pixel level. The proposed scheme has advantages over other schemes because it achieves a better space-frequency resolution and therefore tracks the topographic changes of the scene more accurately. The filters used in this work are modulated Gaussian functions with variable spatial aperture and bandwidth. In this way, the analysis window is adapted to the local characteristics of the signal at all samples. The variable-aperture filters are similar to the variable space-frequency domain filters used in wavelet analysis. We present results on synthetic and real SAR interferograms.

1. INTRODUCTION

For the production of digital elevation models from SAR interferograms to become fully operational, appropriate filtering of the raw interferogram data is necessary. Since the frequency content of the signal changes from point to point, this filtering is space-variant and must be controlled exclusively by the data so that the filtering process is not biased.

For each area in the interferogram, the local spatial frequency is geometrically related to the local terrain slope of the scene [1]. The estimates of the local frequency are used to smooth the interferogram and reduce the phase noise through slope-adaptive filtering [2]. The slope-adaptive filtering is an extension of the multi-look averaging filter, with the additional advantage that the slope is corrected. In the multi-look averaging filter, neighboring pixels are averaged to reduce the noise variance [3], but this also reduces the resolution of the interferogram because neighboring pixels do not necessarily have the same phase. In the slope-adaptive filtering, the estimated local frequency allows us to locally flatten the interferogram before the average is performed.

After adequate filtering, the number of residues confronting the phase unwrapping process are reduced. Clearly, the accuracy of the elevation obtained from the unwrapped phase of the filtered interferogram depends on the accuracy of the frequency estimation.

The frequency estimates are also used to correct the effect of the slope in the coherence estimation. In [2], the authors showed that the estimation of the 2D frequency makes phase unwrapping feasible even for very noisy interferograms. The objective of the present work is to estimate the local frequency with high accuracy and resolution for the applications mentioned above.

Authors in the past have estimated the local frequency of an interferogram after sub-dividing it in windows [4, 5, 6]. They assumed that the signal within each window is stationary, i.e. contains only one dominant frequency. Independently of which technique is used to estimate the frequency, there is a trade-off between the size of the window and the accuracy of the estimation. In order to get estimates that perform well in the presence of noise, the analysis window must be made large. But, the use of large windows when the scene topography is rough will cause large differences between the real Instantaneous Frequency (IF) at each pixel and the estimated frequency assigned to all the pixels in the window.

We propose a method where the spatial frequency is estimated at the pixel level in order to

provide a more accurate representation of the scene topography. To reduce the size of the window without increasing the estimation error, the amount of noise present in the signal is previously reduced through multiband filtering. Therefore, the proposed method consists of two stages: multiband filtering of the interferogram and instantaneous frequency estimation.

For the filtering stage, a set of Gaussian filters with variable spatial aperture and bandwidths is proposed, in order to effectively sample areas of different frequency content.

Each stage of the proposed estimation method is described in Section 2, together with the relation between the proposed method and others based on the STFT (Short Time Fourier Transform). In Section 3, simulations show that the estimation error obtained using the proposed approach is lower than the obtained using other window-based methods, for values of coherence higher than 0.66. The application of the proposed method to real interferograms is shown in Section 4 and conclusions are made in Section 5.

2. PROPOSED METHOD

2.1 General Description

The steps of the proposed method are illustrated in Figure 1. The input signal $s(\underline{x})$ is a processed interferogram after half-band filtering but before flattening. The processing steps are summarized as follows:

i) The input interferogram signal $s(\underline{x})$ is convolved with each filter g_i, and the magnitudes of the filter outputs are compared for each pixel in the image. The comparison process occurs in block MAX where the channel with the highest magnitude is selected.

ii) The instantaneous frequency (IF) is estimated from $y(\underline{x})$ of the MAX output, giving the frequency estimate $\nabla\hat{\Omega}(\underline{x})$ for each pixel $\underline{x}$ in the image.

iii) The estimate $\nabla\hat{\Omega}(\underline{x})$ is used to perform slope-adaptive filtering on the input interferogram (block A in Figure 1) and then phase unwrapping.

Instead of phase unwrapping, the frequency estimates $\nabla\hat{\Omega}(\underline{x})$ could be used to obtain the estimated unwrapped phase $\hat{\Omega}(\underline{x})$ by integration (indicated by B in Figure 1). Only alternative A is considered in this paper.

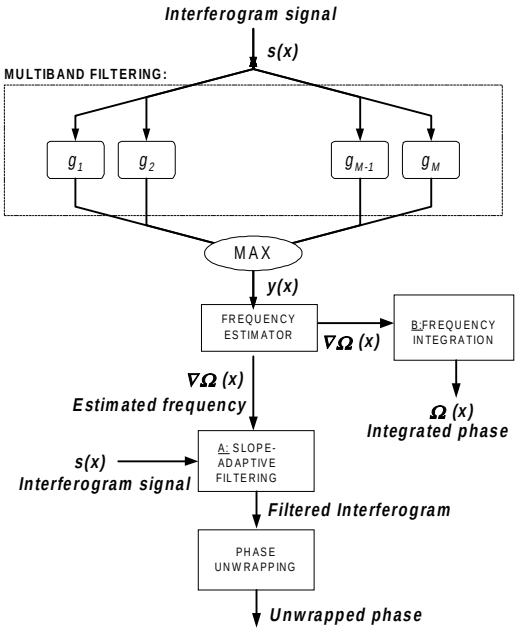

Figure 1: Block Diagram of the Proposed Frequency Estimation Method.

2.2 Selection of the Type of Filters in the Multiband Pre-filtering Stage.

The filtering stage in Figure 1 is named multiband filtering because the half plane of positive range frequencies is covered by the multiple pass-bands of the filters. The output signals of the multiband filters are M channels containing filtered versions of the input signal. After selecting the maximum channel output, an estimation of the instantaneous frequency is obtained for all samples.

The choice of the filters can be arbitrary. The only requirement is that they sample the frequency space densely so the filter including the local frequency has a high response and the other filters receive noise. Because of their space-frequency localization – more specifically the achievement of the lower bound of the uncertainty principle [7] – we use Gaussian filters of the following one-dimensional form:

$$g_i(x) = \frac{1}{\sigma_i\sqrt{2\pi}} e^{-x^2/2\sigma_i^2} e^{j\omega_i x} \qquad (1)$$

with Fourier Transform:

$$G_i(\omega) = e^{-\sigma_i^2(\omega-\omega_i)^2/2} \qquad (2)$$

for $i = 1,2,...,M$, where ω_i is the center frequency

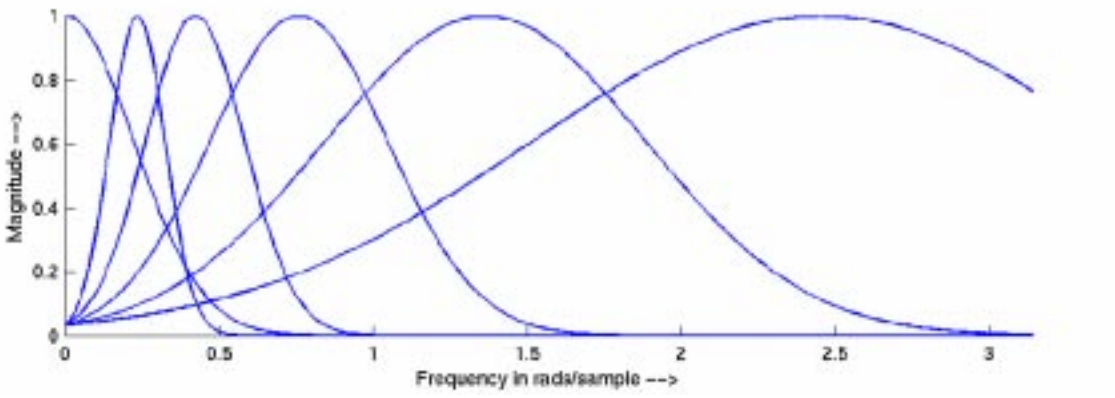

Figure 2(a): Magnitude Spectrum of Gabor filters. All filters have the same shape but are centred at different frequencies in order to cover the interval $[0,\pi)$.

of each filter g_i and σ_i its spatial aperture parameter.

In order to adapt the multiband filtering scheme to the characteristics of low frequency and high frequency events, the filters have variable spatial aperture and variable spatial frequency bandwidth, similar to the variable space-frequency distribution used in wavelet analysis [8]. Figure 2(a) illustrates the magnitude frequency response of 6 Gabor filters in one dimension. The frequency response of each filter is normalized and their main lobes intersect at 75% of the maximum magnitude.

In order to sample the 2D frequency half-plane of positive range frequencies, the filters are rotated each $\pi/8$ rads. as illustrated in Figure 2(b). If the input signal is previously band-pass filtered to its effective global bandwidth, not all the filters in Figure 2(b) are used.

The multiband filtering objective is to densely sample the frequency space of the interferogram signal in order to detect the local bandwidth of the signal. Because half-band filtering has been previously applied to reduce overlay effects [1], only the half plane of positive range frequencies needs to be sampled. On the other hand, by shifting the filters' frequency responses, the scheme can be easily adapted to process flattened interferograms.

2.3 Relation of the proposed method to the STFT

The use of the Short Time Fourier Transform (STFT) in the estimation of local frequency in interferograms has been reported in [5, 6]. The STFT of a signal $x(n)$ is defined by:

$$S_{STFT}(n,w) = \sum_{a} x(a)\, w(n-a)\, e^{-j\omega a} \qquad (3)$$

The squared magnitude of the STFT is an estimate of the periodogram of the signal. The frequency of the peak in the periodogram constitutes a Maximum Likelihood (ML) estimate of the local frequency of the signal [10]. The spatial extent of the window $w(n)$ has an important effect upon the frequency resolution. If a short window is used to compute (3), the transform will exhibit good resolution in space, but the frequency resolution will be low. Alternatively, if a longer window is used in order to increase the frequency resolution, the spatial resolution (localization) will be poor.

The alternative proposed in this work is clearly seen when (3) is expressed as a convolution of the frequency-shifted signal $x(m)e^{-j\omega m}$ with $w(m)$. At a specific sample, (3) can be re-written as:

$$\begin{aligned} S_{STFT}(n,\omega) &= x(n)e^{-j\omega n} * w(n) \\ &= \{x(n) * w(n)e^{j\omega n}\}\, e^{-j\omega n} \end{aligned}$$

$$\left| S_{STFT}(n,\omega) \right| = \left| \{x(n) * h_{\omega}(n)\} \right| \qquad (4)$$

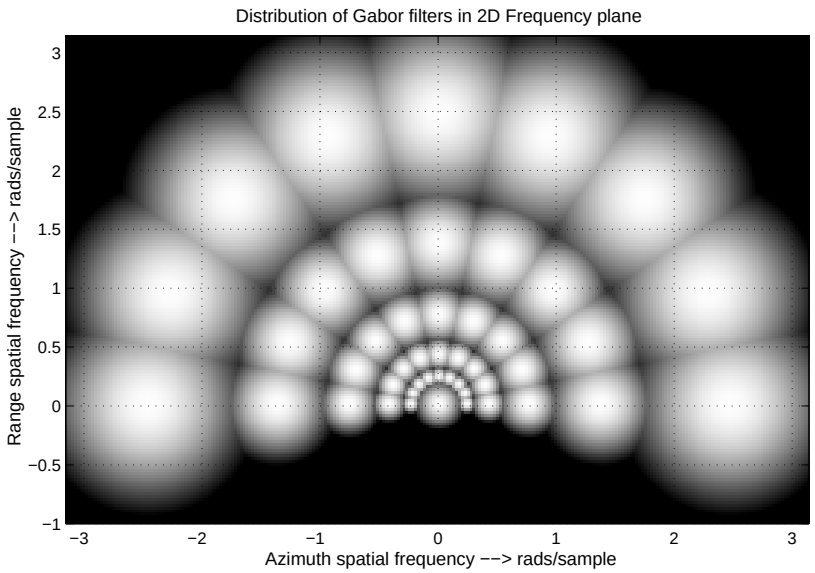

Figure 2(b): Magnitude Spectrum of Gabor filters in the 2D-frequency plane.

If the frequency is held constant $\omega = \omega_o$, then (4) is the magnitude response of a filter h_{ω_o} to an input $x(n)$. The frequency response of h_{ω_o} is $H_{\omega_o}(\omega) = W(\omega - \omega_0)$, which is the same as the window function frequency response shifted to the frequency ω_o.

The analysis above shows that the proposed approach alleviates the problem of poor space-frequency resolution of the STFT, because the window is locally optimized. For instance, a high frequency event is analyzed with a small window and a low frequency event is analyzed with a large window. Thus, by varying the window size and approximately match filtering the signal, the proposed approach applies an appropriate window to the signal at all samples.

The task of finding which window fits the local characteristics of the input best is simplified to finding which filter $h_\omega(n)$ maximizes the output in (4).

Such maximization could be performed over all frequencies ω in the frequency plane. Instead, a much smaller number of filters are used and the Instantaneous Frequency (IF) is estimated at the pixel level on the output $x(n) * h_\omega(n)$ using the DESA-1 algorithm introduced in next section.

2.4 Instantaneous Frequency Estimation

There are many IF estimators that could be used for interferogram signals [11,12]. They have different signal model assumptions and computational complexities. Although the proposed scheme is not restricted to one kind of IF estimator, a simple and efficient IF estimator is considered in this work based on the Energy Separation Algorithm (ESA) [15]. The ESA algorithm was introduced to analyze speech signals from the point of view of the energy required to generate them. In its *discrete* form, the energy tracking operator ψ of the signal $x(n)$ is defined by:

$$\psi\,[x(n)] = x^2(n) - x(n+1)x(n-1), \qquad (5)$$

from which the IF can be obtained by:

$$\Omega_i(n) \;\approx\; \cos^{-1}\left\{1 - \frac{\psi[x(n) + x(n+1)]}{4\psi[x(n)]}\right\} \qquad (6)$$

The DESA-1 (Discrete Energy Separation Algorithm) algorithm described by (6) was chosen to implement the IF estimation in the proposed method because of its low computational complexity compared with other methods of comparable performance. To compute (6), five neighboring samples are used.

3. RESULTS ON SYNTHETIC DATA

Consider a "Gaussian hill" phase interferogram signal $\phi(x, y)$:

$$\phi(x,y) \;=\; K\, e^{-(x-N)^2/\alpha^2}\; e^{-(y-N)^2/9\alpha^2}$$

$$\textit{with}\;\; x,\, y \;=\; 1, \ldots, N \qquad (7)$$

The synthetic interferogram $s_1 s_2^*$ is obtained using the following model [13]:

$$s_1 = ce^{j\phi} + n_1 \quad \text{and} \quad s_2 = c + n_2 \qquad (8)$$

where n_1, n_2 are independent complex random variables with normal distribution, zero mean and variance σ_n^2, and c is the correlated part common to both signals. c is modeled by a complex random variable with normal distribution, zero mean and variance σ_c^2. The interferogram coherence is given by [13]:

$$\mu = \left(1 + \frac{\sigma_n^2}{\sigma_c^2}\right)^{-1} \qquad (9)$$

The signal $s_1 s_2^*$ – illustrated in Figure 3 for $\sigma^2 = 800$ and 0.57 coherence – is convolved with each one of the Gabor filters illustrated in Figure 2(b). As an example of the filtering properties of the proposed scheme, Figures 4(a) and 4(b) illustrate the outputs of two of the Gabor filters. Figure 4(a) illustrates the output of the Gabor filter centered at the second radial frequency and 0 rads/ sample in the azimuth direction. The filter response is of high contrast (high magnitude) in the areas where the frequency and orientation of the input signal correspond to that of the filter, like at the bottom and top of the image.

Figure 4(b) gives the output of the Gabor filter centered at the third radial frequency and 0 rads/ sample in the azimuth direction. Figures 4(a) and (b) complement each other. For instance, at the center of the image the response of the filter in 4(a) is low and in 4(b) is high. Notice that the outputs are smooth in the areas where the magnitude is high, since the out-of-band noise has been filtered out in these regions. In this example most of the signal frequency contents is located in the pass-bands of these two Gabor filters, but in general the frequency content can be located in any part of the frequency half-plane of Figure 2(b).

There are two sources of errors in the IF estimation: i) the noise added to the synthetic signal, and ii) the "distortion" error inherent to the DESA-1 algorithm which is evaluated in [9]. To separate each source of error, consider the IF estimation results on the signal *without noise*. In Figure 5, 1D slices of the estimated IF are drawn with a continuous line and the theoretical IF with a dash-dot line. The 1D slices are done by the center of the image in Figure 3 in the range direction. For the purposes of illustrating the specific channel used at every pixel, the center frequency of the filter with maximum output used to estimate the IF is drawn with a dotted line. Note that the centre frequencies of the filters are heavily quantized, but the estimated frequencies are continuous. Although there is some ripple in the estimation of the IF in Figure 5, the estimation error is quite low when no noise is present.

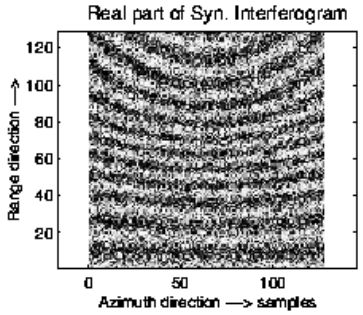

Figure 3: Synthetic interferogram input

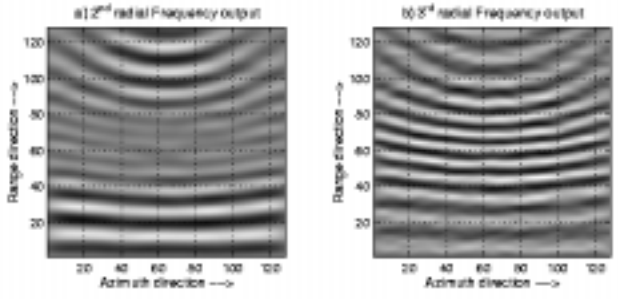

Figure 4: Outputs of two Gabor filters

3.1 IF Estimation Performance.

The distortion error of the DESA-1 algorithm will increase with higher variations of the interferogram IF. This can be simulated by increasing the slope of the Gaussian hill – i.e. decreasing α^2 in (7). Figure 6 illustrates the Mean Square Error (MSE) of the IF estimation vs. interferogram coherence, when the values of α^2 are set between 50 (fast IF variation) and 800 (slow IF variation).

The MSE error in Figure 6 is defined by:

$$\varepsilon_{MSE} = \frac{1}{N}\sum_n \left(\Omega_i(n) - \Omega_{real}(n)\right)^2 \quad (10)$$

where Ω_i is the estimated IF, Ω_{real} is the real IF and N the number of samples in the image.

When the coherence of the simulated interferogram drops below 0.66, the MSE error increases dramatically for all values of α^2. At this value of coherence, the multiband filtering and the MAX block of Figure 1 are not able to locate the local frequency very well due to the larger phase noise.

In order to compare the performance of the proposed method against other window-based IF estimators, consider a hypothetical IF estimator that exactly computes the average of the noise-free signal IF in cells of size A_i^2 pixels. To implement such a IF estimator, the theoretical frequency is averaged in cells of A_i^2 pixels and the resulting IF is assigned to each one of the pixels in the window.

Figures 7(a) to (d) show the estimation error of the hypothetical estimator in dashed lines, superimposed on the curves of Figure 6 for different values of A_i, namely 5,10 and 20 pixels.

For each experiment (value of α^2), the IF estimation error of the proposed method is always less than that obtained by the hypothetical estimator when the averaging window of the hypothetical estimator is large – 10 and 20 pixels. The estimation error is approximately equal for both estimators when A_i is 5 pixels and the coherence is 0.66.

Since the estimated IF of the hypothetical method is computed in the absence of noise, it can be concluded that the error of the IF estimation using the proposed method is less than the obtained by any other window-based method for coherence values higher than 0.66. In other words, a real window-based IF estimator will have estimation errors higher than the plotted in dashed lines in Figure 7.

4. RESULTS ON REAL SAR DATA

Figure 8(a) shows a segment of an ERS Tandem mission interferogram of the Chilcotin area in BC (Canada). Among all the Gabor filter outputs, three have been chosen which show different signal characteristics. Figure 8(b) corresponds to the first radial frequency and an orientation close to the dominant fringe orientation of the image. Figures 8(c) and (d) correspond to two different orientations of the second radial frequency and have high contrast (magnitude) along the valley that crosses the scene. Figures 8(b), (c) and (d) grossly represent the input interferogram, but many other details are represented by other frequency and orientation channels.

The center frequency of the filter whose output magnitude is maximum at each pixel is shown in Figure 9(a), and the magnitude of the estimated IF is shown in Figure 9(b). Lighter shades correspond to high frequencies and darker shades to lower frequencies. The estimated IF in the image varies between 0 and 1.99 rads/sample. Again note how the frequency estimates are finer than the quantization of the filter centre frequencies.

5. CONCLUSIONS

In this work we proposed a method to estimate the IF of an interferogram. Simulations showed that the estimation error achieved by the proposed method is lower than the achieved by any other window-based method for coherence values higher than 0.66. This performance improvement is achieved because of i) the use of highly localized filters that adapt their spatial aperture to local frequency contents of the signal, and ii) the IF is estimated on each pixel of the image.

6. FUTURE WORK

The implementation efficiency may be improved by the use of Kalman filters as proposed in [14], since the frequency content of the signal is spatially correlated.

In addition to the use of the estimated local frequency in phase unwrapping, the ratio between the highest filter magnitude and the neighboring filters' magnitudes can be used as a measure of the local SNR.

As proposed in Section 2.1, it is possible to use the frequency estimates to obtain the unwrapped phase by direct integration, rather than through phase unwrapping. This hypothesis is based on the complete representation that can be achieved of a monochromatic signal by the mono-component AM-FM (Amplitude Modulation Frequency Modulation) model [16]. The main advantage of this alternative is that the IF estimates are a lot less noisy than the filtered phase, creating an alternative to unwrap very noisy interferograms. The field of estimated frequencies is also non-conservative, therefore, similar algorithms to phase unwrapping could be used.

The above implies that future work must be done to adapt the proposed scheme to noisier interferograms (coherence less than 0.66). The

filter parameters that can be varied are: the number of filters and their center frequencies, and the threshold at which their frequency response intersect. The automatic selection of these parameters should be also addressed to reduce user's interaction.

Acknowledgements

Special thanks to Dr. Michael Seymour from MacDonald Dettwiler for his valuable support throughout all the stages of the project. This work was financially supported by MacDonald Dettwiler, NSERC, BC ASI and the Science Council of BC.

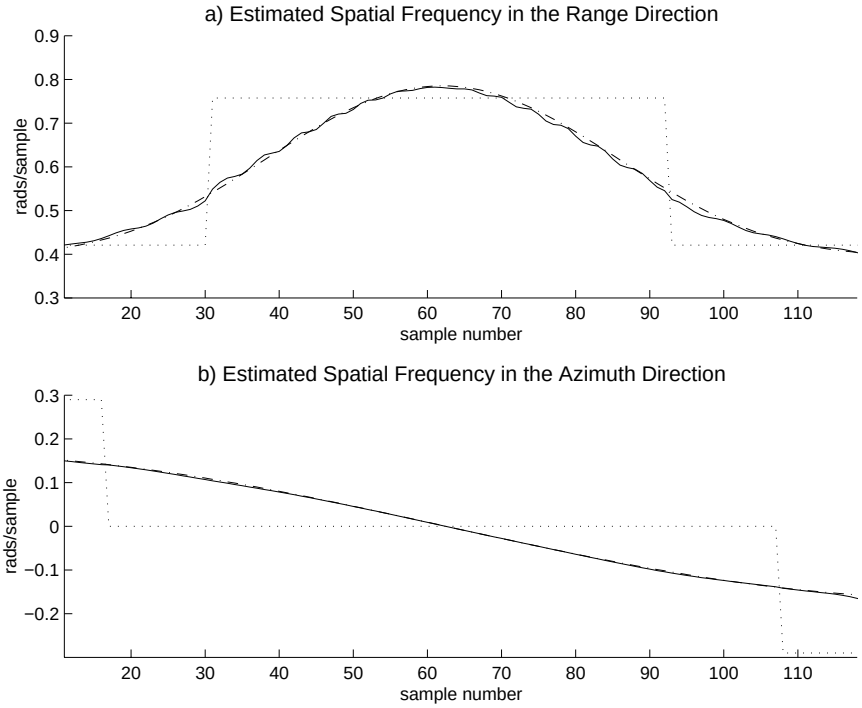

Figure 5: 1D slices of the estimated IF (no noise case)

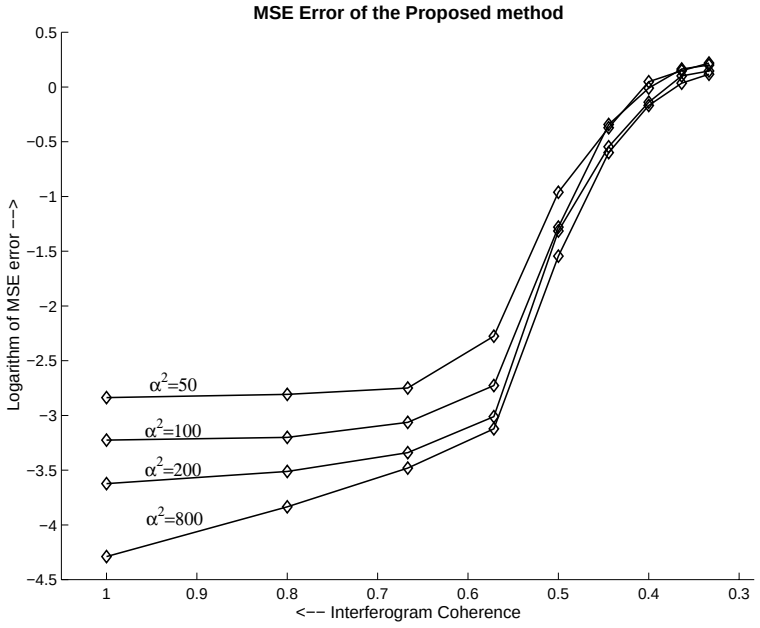

Figure 6: IF estimation error vs. frequency variations and coherence

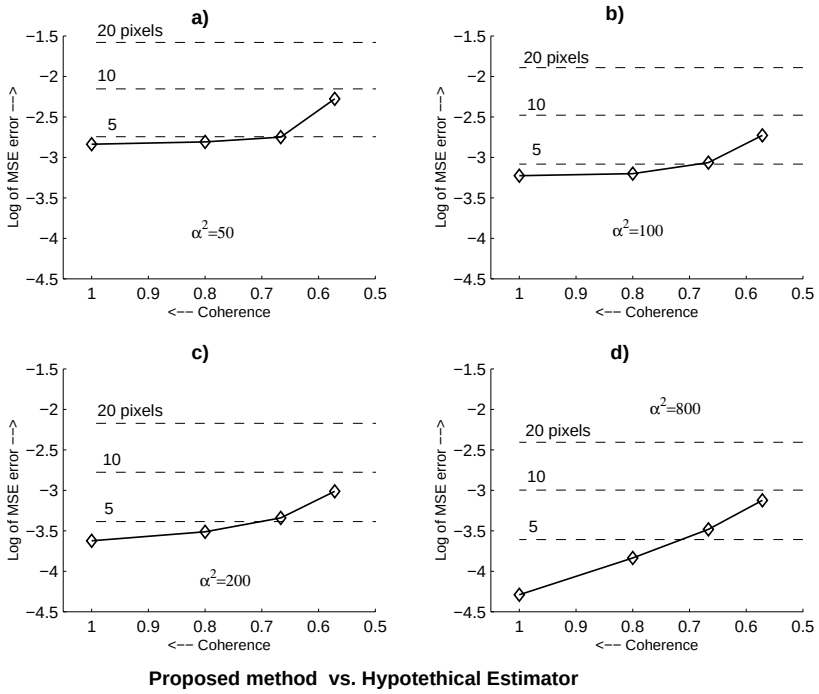

Figure 7: Performance of proposed method (solid line) vs. Hypothetical Estimator (dashed line)

References

[1] F. Gatelli et. al, "The wavenumber shift in SAR interferometry," *IEEE Trans. Geosci Remote Sensing*, vol. 32, pp. 855-865, July 1994.

[2] E. Trouve, J. Nicolas, H. Maitre "Improving phase unwrapping techniques by the use of local frequency estimates", *IEEE Trans. Geosci. Remote Sensing*, vol. 36, pp. 1963-1972, November 1998.

[3] J. Lee et. al, "Intensity and phase statistics of multilook polarimetric and interferometric imagery", *IEEE Trans. Geosci. Remote Sensing*, vol. 32, pp. 1017-1028, September 1995.

[4] E. Trouve, M. Caramma, H. Maitre "Fringe detection in noisy complex interferograms" Appl. Optics, vol. 35, pp. 3799-3806, July 1996.

[5] D. Ghiglia, "IFSAR correlation improvement through local slope correction", in Proc. IGARSS'1998, vol. 5, pp. 2445-2447.

[6] D. Zhu, R. Scheiber, "Smooth the Interferogram and improve the coherence estimation for weighted least square phase unwrapping by local frequency estimation", Deutsches Zentrum f.Luft-u. Raumfahrt (DLR) report, 1999.

[7] Daugman J., "Uncertainty relation for resolution in space, spatial frequency, and orientation optimized by 2D visual cortical filters", J. Opt. Soc. Am., vol. 2 no 7, pp. 1160-1169, July 1985.

[8] I. Daubechies, "The wavelet transform, time-frequency localization and signal analysis", *IEEE Trans. on Information Theory*, vol. 36, pp. 961-975 1005, Septemeber 1990.

[9] D. Perea-Vega, "Local Frequency Estimation in Interferograms", M.A.Sc. thesis, Dept. of Electrical and Computer Eng, University of British Columbia, Canada, November 1999.

[10] A. Papoulis, *Probability, Random Variables, and Stochastic Processes*, McGraw-Hill, Inc. 1991.

[11] U. Spagnolini, "2-D phase unwrapping and instantaneous frequency estimation", *IEEE Trans. Geosci. Remote Sensing*, vol. 33, pp. 579-589, May 1995.

[12] B. Boashash, "Estimating and interpreting the instantaneous frequency of a signal – Part 2: Algorithms and applications", Proc. of IEEE, vol. 80, no. 4, pp. 540-568, April 1992.

[13] H. Zebker and J. Villasenor, "Decorrelation in interferometric radar echoes", *IEEE Trans. Geosci. Remote Sensing*, vol. 30, pp. 950-959, Sept. 1992.

[14] J. Havlicek, A. Bovik, "Multi-component AM-FM image models and wavelet-based demodulation with component tracking", in Proc. IEEE Int. Conf. Image Processing, Austin, TX, Nov. 13-16, 1994, pp. 141-145.

[15] P. Maragos et. al, "Energy separation in signals modulations with application to speech analysis", *IEEE Trans. on Signal Processing*, vol. 41, No. 10, pp. 3024-3051, Oct. 1993.

[16] A. Bovik, P. Maragos, T. Quatieri, "AM-FM energy detection and separation in noise using multiband energy operators", *IEEE Trans. on Signal Processing*, vol. 41, pp. No. 10, pp. 3245-3265, Dec. 1993.

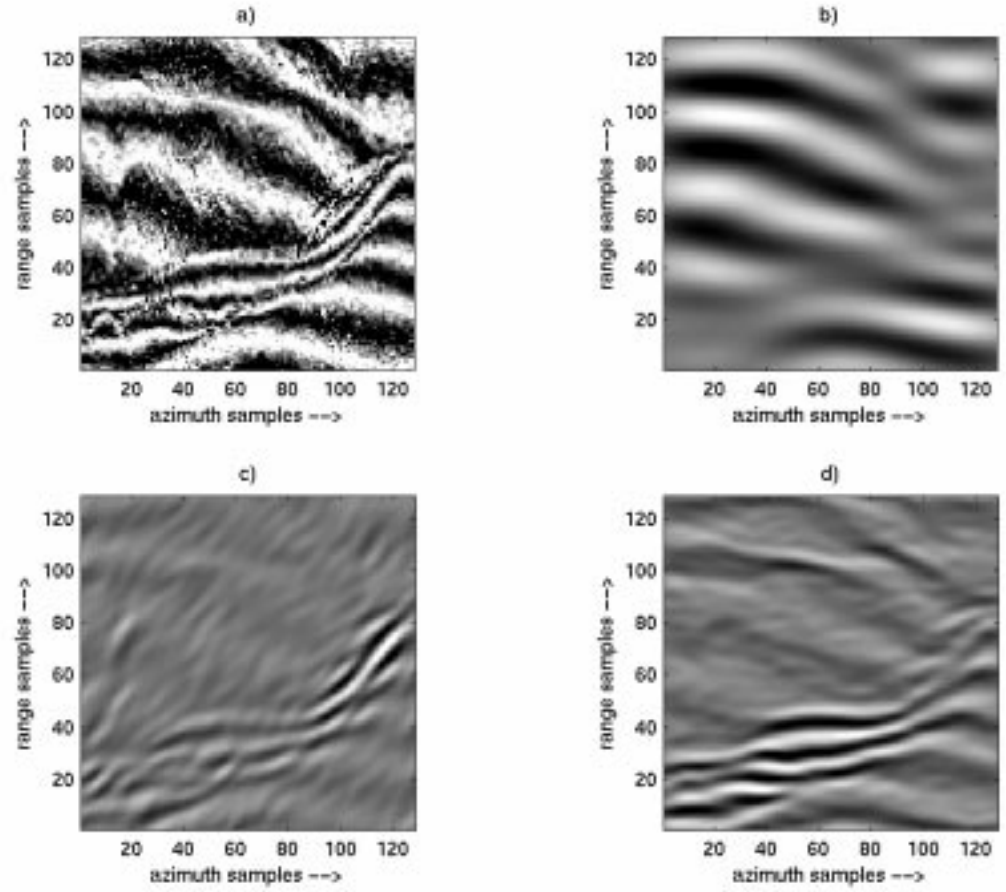

Figure 8: Input interferogram and some Gabor filter outputs

a) Unfiltered ERS SAR interferogram

b)-d) Three Gabor filter outputs.

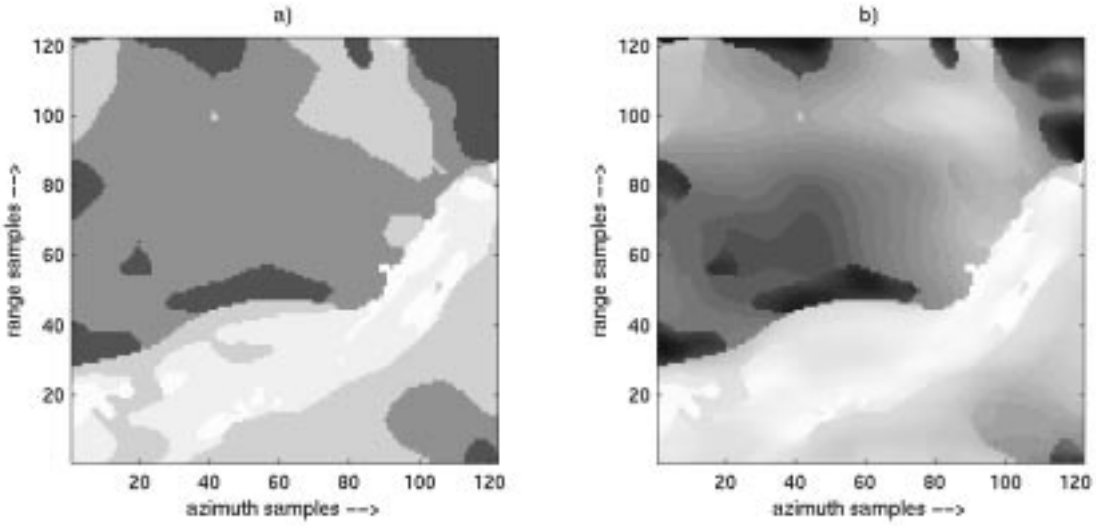

Figure 9: Frequency estimation results on the SAR interferogram

a) Magn. of filter center frequencies *b) Magnitude of estimated IF*